$R'' \neq H$, the ester channel apparently cannot compete with the hydroperoxide channel. Our modeling studies suggest this may be true for TME and possibly also for isobutene, propene, and 2-butene. If correct, then atmospheric models will have to be modified to account for this significantly greater reactivity in ozonolysis reactions.

The secondary reactions included in the computer model can account for the stoichiometry observed in the gas-phase O_3 + TME reaction. This reaction appears to proceed through the hydroperoxide and hydroxyacetone, as it does in solution. Moreover, the computer simulation and the zeroth-order thermochemical kinetics estimates suggest that hydroxyacetone and methylglyoxal are both "prompt" products resulting from sequential isomerizations subsequent to the formation of the Me_2COO.

Registry No. TME, 563-79-1.

Pulse Radiolytic Investigations of Aqueous Solutions of Methoxybenzene Cation Radicals: The Effect of Colloidal RuO_2

Marek Brandys,† Richard E. Sassoon,‡ and Joseph Rabani*

Energy Research Center and The Department of Physical Chemistry, The Hebrew University of Jerusalem, Jerusalem 91904, Israel *(Received: August 1, 1985; In Final Form: September 11, 1986)*

The formation and decay of the radical cations of 1,4-dimethoxybenzene (DMB) and 1,2,4,5-tetramethoxybenzene (TMB) were investigated by the pulse radiolysis technique in the absence and the presence of colloidal RuO_2 particles. $DMB^{\bullet+}$ was obtained only by Tl^{2+} oxidation of DMB while $TMB^{\bullet+}$ was produced by oxidation of TMB using both Tl^{2+} and Br_2^-. In the absence of RuO_2 both $DMB^{\bullet+}$ and $TMB^{\bullet+}$ decay predominantly via a second-order process, although there is a contribution of a pseudo-first-order reaction. The rate constants for these reactions are reported. RuO_2 colloidal particles catalyze the decay of both $TMB^{\bullet+}$ and $DMB^{\bullet+}$. The reactions of $TMB^{\bullet+}$ with RuO_2 were found to depend on pH, pulse intensity, and colloid concentration. At pH 3–4, adsorption of $TMB^{\bullet+}$ to the colloid is observed, followed by the decay of the remaining $TMB^{\bullet+}$ in the bulk. At higher pHs, loading of the RuO_2 colloid by positive holes takes place until equilibrium is achieved between loaded holes and $TMB^{\bullet+}$ and again the remaining $TMB^{\bullet+}$ decays at a later stage. The fraction of $TMB^{\bullet+}$ that loads the colloidal particles increases with both pH and $[RuO_2]$. It is also suggested that $DMB^{\bullet+}$ loads the RuO_2 at the pH where experiments were performed. $(TMB)_2$ and $(DMB)_2$ dimers (or higher oligomers) are suggested to be the final products both in the absence and presence of RuO_2. No O_2 is formed with the RuO_2 colloid despite a favorable redox potential for water oxidation.

Introduction

Alkoxybenzenes are known to be good electron donors and may serve as quenchers in photoinduced electron-transfer systems.[1] For example 1,4-dimethoxybenzene (DMB) and 1,2,4,5-tetramethoxybenzene (TMB) possess many ideal properties that may make them suitable as positive hole relays in catalytic light-energy conversion systems. They have high positive redox potentials ($E^\circ_{DMB^{\bullet+}/0} = 1.59$ V, $E^\circ_{TMB^{\bullet+}/0} = 1.06$ V vs. NHE[2]) and relatively high solubilities in water (slightly less than 10^{-2} M) and produce relatively stable cation radicals.[3-5] Both have been shown to quench various photosensitizers such as acridine orange,[6] $Ir(bpy)_2(Hbpy\text{-}C^3,N^1)^{3+}$,[7] and UO_2^{2+}[8] at nearly diffusion-controlled rates. Several methoxybenzenes have also been found to quench a polypyridylruthenium derivative as a photosensitizer.[9] It was shown that in acetonitrile oxidative quenching takes place with rates 2–3 orders of magnitude slower than those that are diffusion controlled. The lifetimes of the photochemical products are, however, relatively short.

The methoxybenzenes used in this work were therefore considered to be very suitable as model systems for oxidizing relays in which they can transfer positive charge either to an appropriate catalyst or to an added donor species in solution. Several investigations[3-5] have already been carried out in order to study the nature of the methoxy radical cations, and hence the aim of our work is to fully understand the nature of oxidized DMB and TMB radicals by using the pulse radiolytic technique and to investigate their decay in the presence of a colloidal RuO_2 catalyst in order to probe the role of RuO_2 as a catalyst for water oxidation.

Experimental Section

Materials. 1,4-Dimethoxybenzene (Aldrich) was recrystallized once from methanol, and 1,2,4,5-tetramethoxybenzene was prepared with minor modifications according to the literature method[10] and gave good microanalysis results after threefold recrystallization from water. Since tetramethoxybenzene solutions were found to decompose during prolonged storage of more than several days, as indicated by changes in their absorption spectra, only freshly prepared solutions were used. The cation radicals were generated by the pulse radiolysis technique in N_2O-saturated solutions containing either Tl_2SO_4 (BDH) or NaBr (Baker analyzed). Buffers consisted of standard pH control solutions.[11] All other reagents were of the highest purity available and were used without further treatment while water was distilled and passed

† Present address: Vitreous State Laboratory, Keane Hall, The Catholic University of America, Washington, D.C. 20064.

‡ Present address: Radiation Laboratory, University of Notre Dame, Notre Dame, Indiana 46556.

(1) Ballardini, R.; Varani, G.; Balzani, V. *J. Am. Chem. Soc.* **1980**, *102*, 1719.
(2) Mann, C. K.; Barnes, K. K. *Electrochemical Reactions in Non-Aqueous Systems*, Marcel Dekker: New York, 1970.
(3) O'Neill, P.; Steenken, S.; Schulte-Frohlinde, D. *Angew. Chem., Int. Ed. Engl.* **1975**, *14*, 430.
(4) O'Neill, P.; Steenken, S.; Schulte-Frohlinde, D. *J. Phys. Chem.* **1975**, *79*, 2773.
(5) Sullivan, P. D.; Brelte, N. A. *J. Phys. Chem.* **1975**, *79*, 474.
(6) Vogelmann, E.; Rauscher, W.; Kramer, H. E. A. *Photochem. Photobiol.* **1979**, *29*, 771.
(7) Slama-Schwok, A.; Rabani, J., to be published.
(8) Brandeis, M.; Sassoon, R. E.; Rabani, J. *Int. Conf. Photochem. Convers. Storage Solar Energy, 5th*, **1984**, Paper A76(1).
(9) Monserret, K.; Foreman, T. K.; Graetzel, M.; Whitten, D. G. *J. Am. Chem. Soc.* **1981**, *103*, 6667.
(10) (a) Benington, F.; Morin, R. D.; Clark, L. C. *J. Org. Chem.* **1955**, *20*, 102. (b) Veda, M.; Sakai, N.; Imai, Y. *Makromol. Chem.* **1979**, *180*, 2813.
(11) Dean, J. A., Ed. *Lange's Handbook of Chemistry*, McGraw Hill: New York, 1979; Tables 5-23, pp 5.77–5.78.

0022-3654/87/2091-0953$01.50/0

through a Millipore Milli-Q water purification system. Colloidal RuO_2 solutions were prepared in the following way:[12] 0.5 g of RuO_4 (Alfa-Ventron) in 100 mL of water was added to 125 mL of a 0.2% solution of sodium poly(styrene-*co*-maleate) at pH 9 with stirring over a period of 1 h. (The copolymer was prepared according to a modified literature procedure[13]). Under these conditions, RuO_4 decomposes spontaneously, yielding the hydrated form of RuO_2. The resulting solution was dialyzed 3 times against 5 L of water, and final dilution up to 0.5 L gave a stock solution with a formal concentration of 6.0 mM RuO_2 and 0.05% stabilizer. The diameter of the RuO_2 colloidal particles was determined to be 350 ± 50 Å from light-scattering measurements using solutions of colloidal TiO_2 obtained by sonication of TiO_2 powder (anatase, type P25, particle size 300 Å, product of Degussa, West Germany) as a reference. Aging of the RuO_2 solutions for several months has only a small, if any, effect on the experimental results.

Apparatus. Absorption spectra were recorded on a Bausch and Lomb Model Spectronic 2000 spectrophotometer. The pulse radiolysis setup consisted of a Varian V7715 linear accelerator fitted with optical detection and computerized data processing systems. The basic features of the system have already been described.[14] The pulse duration varied from 0.1 to 1.5 μs with a dose ranging from 0.2 to 3.5 krad. Dosimetry was performed with N_2O-saturated $Fe(CN)_6^{4-}$ solutions taking $G(Fe(CN)_6^{3-}) = G_e + G_{OH} = 6$ and $\epsilon^{420}_{Fe(CN)_6^{3-}} = 1000\ M^{-1}\ cm^{-1}$. Steady-state irradiations were performed with a Cs-137 γ source (Radiation Machinery Corp.) and the absorbed dose rate was 1.5 krad/min. All experiments were carried out at a temperature of 22 ± 2 °C.

In the absence of RuO_2, reaction rate constants could be determined with an accuracy of ±10% and in the presence of RuO_2 within ±15% when the colloid preparation procedure was strictly followed. Only when an acetate buffer was used for pH control (pH 4–5) did the reproducibility of the results become lower (±20%) and the rates of the decay in the presence of RuO_2 were about 50% higher than those in the absence of buffer, possibly due to specific interactions between acetate ions and the colloidal particles. Cyclic voltammetric measurements on a 5×10^{-3} M solution of TMB were performed in aqueous solution at a platinum disk working electrode with 0.1 M $NaClO_4$ as the supporting electrolyte.

Results and Discussion

Part A: Oxidation of Dimethoxybenzene and Tetramethoxybenzene and the Decay of Their Cation Radicals. Production of Methoxybenzene Radicals. Direct oxidation of methoxybenzenes by OH radicals cannot be achieved since their OH adducts are formed.[4] For example the formation of TMBOH as given by eq 1 ($\epsilon^{447}_{TMBOH} = 2200\ M^{-1}\ cm^{-1}$) was found to follow

$$OH + TMB \rightarrow TMBOH \quad (1)$$

a pseudo-first-order rate law in the presence of 1×10^{-5} M TMB and occurs with a second-order rate constant of $(7 \pm 1) \times 10^9\ M^{-1}\ s^{-1}$. Although in acid pH the OH adducts of methoxybenzenes are quickly converted to the cation radicals (also see later) we preferred to generate the methoxybenzene cation radicals by oxidation by either Tl^{2+} or Br_2^-.

Oxidation by Tl^{2+}. Tl^{2+} is produced on irradiating N_2O-saturated solutions of Tl^+ at pH 4 according to the following reaction sequence:[4]

$$H_2O \rightsquigarrow H_2, H_2O_2, H, OH, e^-_{aq}, H_3O^+_{aq}, OH^-_{aq} \quad (2)$$

$$e^-_{aq} + N_2O \xrightarrow{H_2O} OH + OH^- + N_2 \quad (3)$$

$$OH + Tl^+ \rightarrow OH^- + Tl^{2+} \quad (4)$$

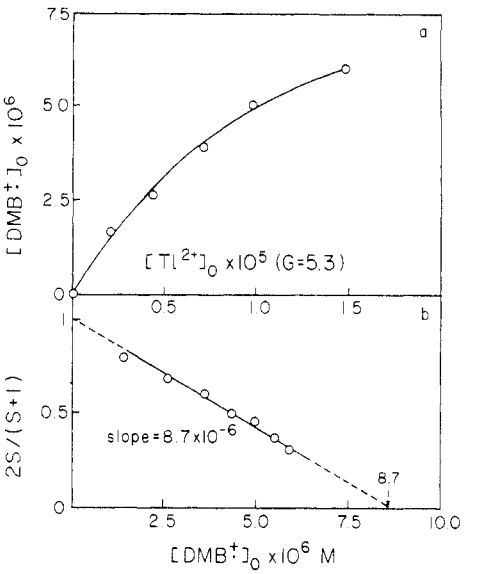

Figure 1. Dependence of $[DMB^{\bullet+}]_0$ on pulse intensity. Data obtained at 460 nm for [DMB] = 1.0×10^{-4} M, $[Tl_2SO_4] = 1 \times 10^{-3}$ M at pH 3.8. $\epsilon^{460}_{DMB^{\bullet+}} = 9540\ M^{-1}\ cm^{-1}$ was used for the calculations of $[DMB^{\bullet+}]_0$. See text for the meaning of S.

Tl^{2+} then undergoes a disproportionation reaction according to eq 5 with a rate constant of $2k_5 = 3.8 \times 10^8\ M^{-1}\ s^{-1}$.[15] When

$$2Tl^{2+} \rightarrow Tl^+ + Tl^{3+} \quad (5)$$

TMB or DMB (in the following, MB) is also present, Tl^{2+} may react according to eq 6. The value of k_6 for TMB was measured

$$Tl^{2+} + MB \rightarrow Tl^+ + MB^{\bullet+} \quad (6)$$

to be $(1.0 \pm 0.1) \times 10^9\ M^{-1}\ s^{-1}$ by following the buildup of the absorption signal of $TMB^{\bullet+}$ at 447 nm in N_2O-saturated solutions containing 1×10^{-4} M TMB and 1×10^{-3} M Tl_2SO_4 at pH 4. A pseudo-first-order reaction was observed and the extinction coefficient of $TMB^{\bullet+}$ at this wavelength was also determined to be $6900\ M^{-1}\ cm^{-1}$ with a value for $G_{TMB^{\bullet+}} = 5.1$.

The formation of $DMB^{\bullet+}$ was followed in the 430–460-nm range where $DMB^{\bullet+}$ possesses two absorption maxima: $\epsilon^{430} = 9040$ and $\epsilon^{460} = 9540\ M^{-1}\ cm^{-1}$.[4] A value of $(5.2 \pm 0.6) \times 10^8\ M^{-1}\ s^{-1}$ was determined for the second-order rate constant for the oxidation of DMB by Tl^{2+}, this being in good agreement with a previously reported value.[4] However, the G value for the production of $DMB^{\bullet+}$ was found to depend on the pulse intensity (Figure 1) and this is attributed to the catalysis of Tl^{2+} disproportionation by $DMB^{\bullet+}$ according to eq 7 and 8. The net result

$$Tl^{2+} + DMB \rightarrow Tl^+ + DMB^{\bullet+} \quad (7)$$

$$Tl^{2+} + DMB^{\bullet+} \rightarrow Tl^{3+} + DMB \quad (8)$$

of these reactions is reaction 5. At high pulse intensities reaction 8 is favored and hence the net $DMB^{\bullet+}$ production is reduced. It can readily be shown that the linear relationship of eq 9 should

$$\frac{2S}{S+1} = -\frac{1}{C}[DMB^{\bullet+}]_{net} + 1 \quad (9)$$

exist for the above reaction sequence, where S is defined as $d[DMB^{\bullet+}]_{net}/d[Tl^{2+}]$, $[DMB^{\bullet+}]_{net}$ is the net concentration of $DMB^{\bullet+}$, $[Tl^{2+}]$ is the initial Tl^{2+} concentration produced according to reaction 4, and C is the ratio $k_7[DMB]/k_8$. Note that $[DMB^{\bullet+}]_{net}$ varies with the pulse intensity, which is proportional to $[Tl^{2+}]$. A plot of $2S/(S+1)$ vs. $[DMB^{\bullet+}]_{net}$ does indeed yield a straight line (Figure 1) and from the slope a value of k_7/k_8 of 8.7×10^{-2} is evaluated. The rate constant, $k_7 = (5.2 \pm 0.6) \times 10^8\ M^{-1}\ s^{-1}$, was measured from the initial rate of $DMB^{\bullet+}$ for-

(12) Kalyanasundaram, K.; Micic, O.; Pramauro, E.; Graetzel, M. *Helv. Chim. Acta* **1979**, *62*, 2432.

(13) (a) Seymour, R. B.; Harris, F. F.; Branum, I. *Ind. Eng. Chem.* **1949**, *41*, 1509. (b) Brandeis, M. Ph.D. Thesis, Hebrew University of Jerusalem, Jerusalem, Israel, 1985.

(14) (a) Zehavi, D.; Rabani, J. *J. Phys. Chem.* **1972**, *76*, 312. (b) Sassoon, R. E. Ph.D. Thesis, Hebrew University of Jerusalem, Jerusalem, Israel, 1983.

(15) Schwarz, H. A.; Comstock, D.; Yandell, J. K.; Dodson, R. W. *J. Phys. Chem.* **1974**, *78*, 488.

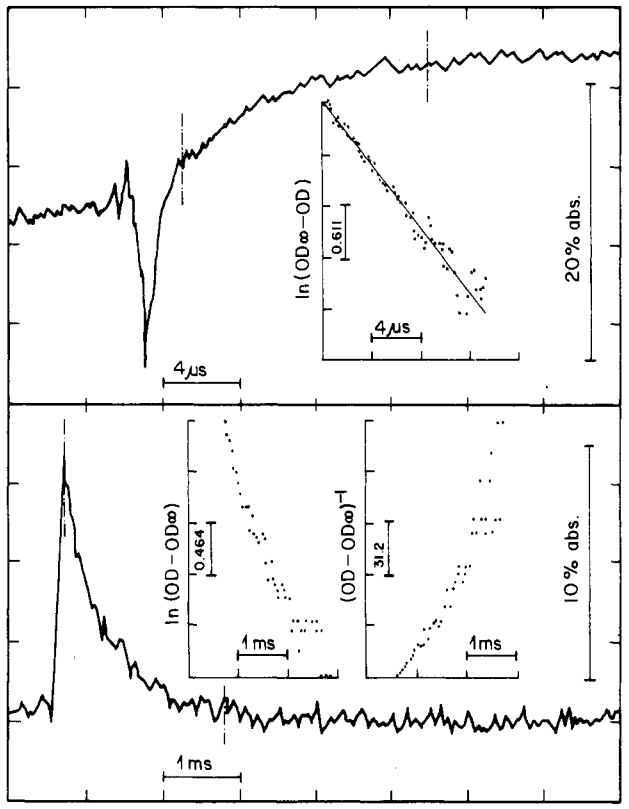

Figure 2. Buildup and decay of the absorption signal of TMBH at 447 nm. [TMB] = 1×10^{-4} M, [*t*-BuOH] = 1×10^{-2} M, pH 2.0. Initial TMBH = 2.4 μM, based on $G_{TMBH} = 3.7$.

mation and hence we obtain $k_8 = (6.0 \pm 1.2) \times 10^9$ M^{-1} s^{-1}. Unlike $[DMB^{\bullet+}]_{net}$, $[TMB^{\bullet+}]_{net}$ does not depend on the pulse intensity, indicating that a reaction analogous to reaction 8 is not important in the TMB system, probably due to the relative redox potentials of $TMB^{\bullet+}$ and Tl^{2+}.

The thallium system can only be utilized at pHs below pH 4. Above this pH, hydrolysis of Tl^{2+} occurs with formation of $TlOH^+$ ($pK = 4.6$[16]) and $TlOH^+$ reacts with methoxybenzenes to yield both the cation radical and the OH adduct.[3] Hence oxidation by a different method was used at higher pHs as described below.

Oxidation by Br_2^-. Br_2^- radical ions react with TMB but not with DMB, and reactions 10 and 11 account for the oxidation reaction in N_2O-saturated solutions containing TMB and Br^-. The

$$OH + Br^- \overset{Br^-}{\rightleftharpoons} OH^- + Br_2^- \quad (10)$$

$$Br_2^- + TMB \rightarrow TMB^{\bullet+} + 2Br^- \quad (11)$$

reaction product possesses an absorption spectrum that is identical with that produced by Tl^{2+}, and we therefore identify the product as $TMB^{\bullet+}$.

The redox potential of Br_2^- ($E^\circ = 1.7$ V vs. NHE[17]) is not sufficiently high for the oxidation of DMB. Indeed under our experimental conditions the decay of Br_2^-, as monitored at 380 nm, was unaffected by the presence of DMB. The reaction rate constant $k_{11} = (1.9 \pm 0.2) \times 10^9$ M^{-1} s^{-1} was determined from the formation rate of $TMB^{\bullet+}$ measured at 447 nm. The *G* value of $TMB^{\bullet+}$ is found to be 6, in agreement with the above reaction sequence. Note that in both the Tl^{2+} and Br_2^- systems the methoxybenzenes also react with H atoms according to reaction 12

$$H + MB \rightarrow MBH \quad (12)$$

to yield an H adduct[4] with $\epsilon^{447}_{TMBH} = 2800$ M^{-1} cm^{-1} and $\epsilon^{460}_{DMBH} < 400$ M^{-1} cm^{-1}. The formation and decay of TMBH at pH 2 in the presence of 1×10^{-2} M *tert*-butyl alcohol are shown in

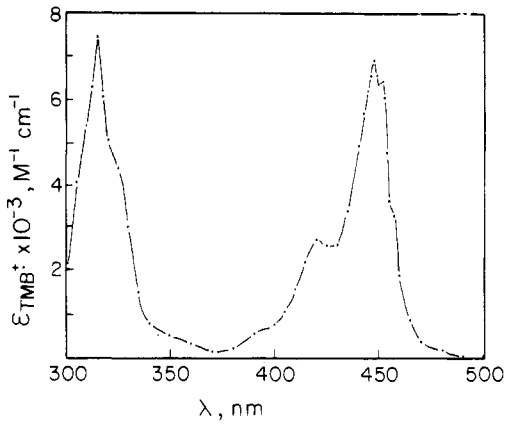

Figure 3. Transient absorption spectrum of $TMB^{\bullet+}$ measured 90 μs after the pulse, 1×10^{-4} M TMB, 1×10^{-3} M Tl_2SO_4, pH 3.8.

Figure 2. The broken vertical lines on this and other figures, presenting decays of absorption signals with time, represent the limits between which kinetics were calculated. k_{12} was determined to be $(1.7 \pm 0.5) \times 10^9$ M^{-1} s^{-1} and the decay of TMBH followed complex kinetics.

The transient absorption spectrum recorded approximately 90 μs after pulse irradiation of an N_2O-saturated solution containing 1×10^{-4} M TMB, 1×10^{-3} M Tl_2SO_4 at pH 3.8 is shown in Figure 3. This is predominantly due to the production of $TMB^{\bullet+}$ with only very minor contributions to the spectrum by TMBH and TMBOH. The following absorption peaks were therefore noted in the spectrum of $TMB^{\bullet+}$: $\epsilon^{452} = 6400$, $\epsilon^{447} = 6900$, $\epsilon^{420} = 2600$, and $\epsilon^{315} = 7400$ M^{-1} cm^{-1}. The absorption spectrum of $DMB^{\bullet+}$ has been reported previously[4] and possesses an absorption maximum at 460 nm ($\epsilon = 9540$ M^{-1} cm^{-1}). The extinction coefficient of TMBH was determined to be 2800 M^{-1} cm^{-1} at 447 nm on pulse radiolysis of a helium-saturated solution containing 1×10^{-4} M TMB, 1×10^{-2} M *tert*-butyl alcohol, and 1×10^{-2} M $HClO_4$ in which TMBH is formed with a *G* value of 3.25. The extinction coefficient of TMBOH was also determined at 447 nm on irradiation of an N_2O-saturated solution containing 1×10^{-5} M TMB at neutral pH. In such a solution TMBOH is produced with a *G* value of 6, and a value for ϵ^{447}_{TMBOH} of 2200 M^{-1} cm^{-1} is obtained. Absorption data on the H and OH adducts of DMB have been noted previously.[4]

Disappearance of the Radical Cations, $DMB^{\bullet+}$ and $TMB^{\bullet+}$. The transient absorption signals observed above 300 nm following production of $DMB^{\bullet+}$ and $TMB^{\bullet+}$ are found to decay over about 200 s to yield residual absorptions of about 7–10% of the original signals, and these residual absorptions disappear over a period of about 30 min. The form of the decay curve varies somewhat with pH, and a description of the decays together with a proposed mechanistic scheme to explain them are described below.

Decay of $DMB^{\bullet+}$ at pH 4 and of $TMB^{\bullet+}$ at pH 3.5–9. The decays of the $MB^{\bullet+}$ radical ions were found to obey mixed second- and first-order kinetics in the first stage of the decay representing approximately 90% of the total decay, and the deviations from a second-order rate law are seen in Figure 4. Furthermore the second-order rate constants, determined from the initial parts of the decay profiles, decrease with increasing pulse intensity (Figure 5) indicating that the first-order contribution is important even in the initial stages of the decay. We believe that the decay of the $MB^{\bullet+}$ radical cation at these pHs can be represented by the reactions given in Scheme I.

$MB^{\bullet+}$ may disappear via one of three pathways: (a) a dimerization reaction with another $MB^{\bullet+}$ species (reaction 13) to yield a stable dimer $(MB)_2$ on the loss of two protons, (b) a reaction with MB itself to yield the species $(MB)_2^{\bullet}$ and a proton (reaction 14), and (c) a reaction with the hydrogen atom adduct MBH to yield unidentified products (reaction 15). Oxidation of the molecular H_2O_2 by $TMB^{\bullet+}$ is thermodynamically unfavorable. Although $DMB^{\bullet+}$ is capable of oxidizing H_2O_2, the similarity of the results observed with both DMB and TMB suggests that H_2O_2 is probably unreactive in the MB systems. Reaction 13 will give

(16) O'Neill, P.; Schulte-Frohlinde, D. *J. Chem. Soc., Chem. Commun.* **1975**, 387.
(17) Henglein, A. *Radiat. Phys. Chem.* **1980**, *15*, 151.

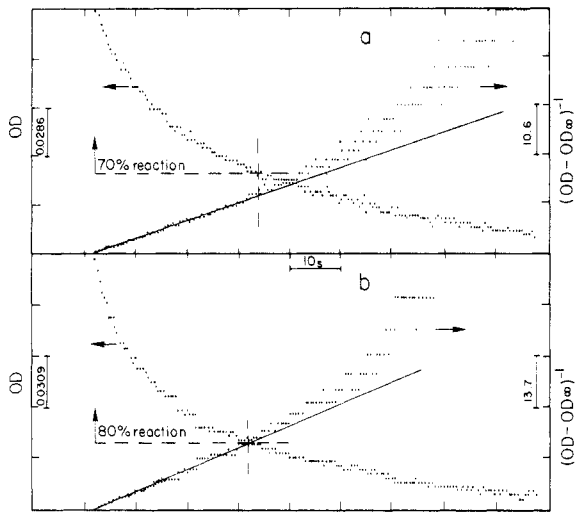

Figure 4. Decay of the absorption signals of the methoxybenzene cation radicals. (a) $DMB^{\bullet+}$ at 460 nm. [DMB] = 1.0×10^{-4} M, $[Tl_2SO_4]$ = 1×10^{-3} M, pH 3.8. Total radical concentration per pulse = 1.85×10^{-5} M. $G_{DMB^{\bullet+}} = 2.15$. (b) $TMB^{\bullet+}$ at 447 nm. [TMB] = 2×10^{-4} M, $[Br^-]$ = 2×10^{-2} M, pH 7.2. Total radical concentration per pulse = 1.85×10^{-5} M. $G_{TMB^{\bullet+}} = 6$.

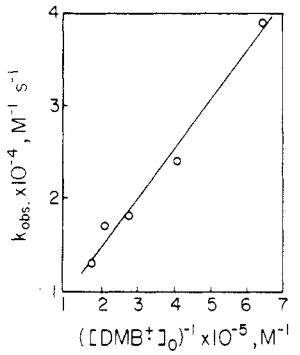

Figure 5. Dependence of the $DMB^{\bullet+}$ decay on its initial concentration. Wavelength = 460 nm, [DMB] = 1×10^{-4} M, $[Tl_2SO_4]$ = 1×10^{-3} M, pH 3.8.

SCHEME I

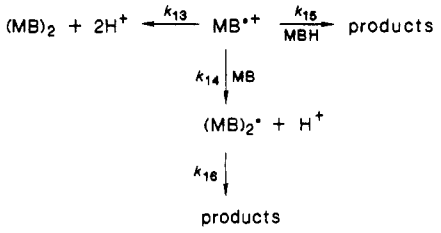

second-order kinetics, whereas reactions 14 and 15 will give pseudo-first-order kinetics and hence the overall decay of $MB^{\bullet+}$ is seen to follow a mixed first- and second-order rate law. The residual absorption of 7–10% of the original $MB^{\bullet+}$ signal found for both DMB and TMB is attributed mainly to the absorption of $(MB)_2^{\bullet}$ which decays very slowly via reaction 16 to yield final products.

Strict second-order kinetics will be observed if reaction 13 is the only pathway for the decay of $MB^{\bullet+}$, and in a previous study[4] second-order kinetics have been reported for the decay of a series of six different methoxybenzene radical cations, not including $TMB^{\bullet+}$. However, both $DMB^{\bullet+}$ and $TMB^{\bullet+}$ possess relatively long lifetimes compared to the other methoxybenzene radicals studied and we suggest that the first-order component of the decay rates is related to the long lifetime of the radical cations, such that the side reactions 14 and 15 become more important, and that the other five methoxybenzene radical cations do indeed decay via a strict second-order reaction. This assumption is supported by experiments that we carried out with 1,3,5-trimethoxybenzene,

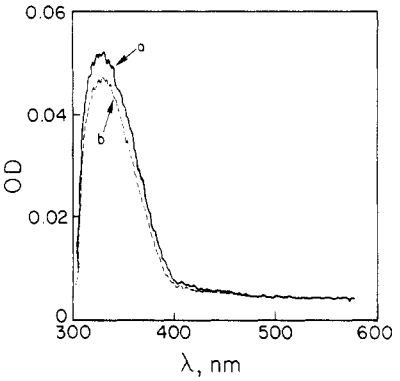

Figure 6. Spectra of final products of irradiation of TMB solutions. [TMB] = 8×10^{-4} M, $[Br^-]$ = 3.2×10^{-2} M, pH 7.0. Total absorbed dose = 8.9 krad: (a) Pulse irradiated; (b) γ-irradiated.

TABLE I: Kinetic Behavior of $TMB^{\bullet+}$ at Higher pH[a]

pH	F^b	slope,[c,d] s^{-1}	slope,[c,e] s^{-1}
<9.2	0.15	0.40 ± 0.07	0.26 ± 0.05
10.1	0.29	3.70 ± 0.60	2.30 ± 0.40
11.1	0.48	36.00 ± 6.00	24.00 ± 4.00

[a] $TMB^{\bullet+}$ was produced on pulse irradiation of an N_2O-saturated solution of 2×10^{-2} M Br^- and 5×10^{-4} M TMB. [b] Fraction of absorption signal that decays during the faster stage via processes I, II, and III. Error is ±0.02. [c] Slopes determined from plots of $(OD)^{-1}$ vs. time at 447 nm, for the slower stage. k_{obsd} can be obtained by multiplying the slopes by $\epsilon^{447}_{TMB^{\bullet+}}$ (6900 M^{-1} cm^{-1}) times l (3 cm). [d] $[TMB^{\bullet+}]_0$ = $(1.0 \pm 0.1) \times 10^{-5}$ M. [e] $[TMB^{\bullet+}]_0$ = $(1.9 \pm 0.1) \times 10^{-5}$ M.

the radical cation of which decays in the millisecond time range, and the decay was found to obey a strict second-order rate law as claimed previously.[4]

If we assume that the first-order component in the decay of $MB^{\bullet+}$ is due mainly to reaction 14, the above mechanism leads to eq 17, where k_{obsd} is defined as the initial $\epsilon_{MB^{\bullet+}} l(d(1/OD)/dt)$

$$k_{obsd} = k_{14}\left\{1 - \frac{\epsilon_{(MB)_2^{\bullet}}}{\epsilon_{MB^{\bullet+}}}\right\}\frac{[MB]}{[MB^{\bullet+}]_0} + 2k_{13} \qquad (17)$$

and $[MB^{\bullet+}]_0$ is the initial concentration of the radical cation. Both k_{13} and k_{14} may be derived on plotting k_{obsd} as a function of $[MB^{\bullet+}]_0^{-1}$ and an example of such a plot for DMB is shown in Figure 5. The results yield $2k_{13} = 3.9 \times 10^3$ M^{-1} s^{-1} and 3.3×10^3 M^{-1} s^{-1} and $k_{14}\{1 - (\epsilon_{(MB)_2^{\bullet}}/\epsilon_{MB^{\bullet+}})\} = 530$ and $70 M^{-1}$ s^{-1} for DMB and TMB respectively, the accuracy of these determinations being ±20%. An accurate determination of k_{14} cannot be made due to the error in the residual absorption.

The difference absorption spectrum observed in TMB–Br^-–N_2O solutions at pH 7, 30 min after applying three pulses yielding a total of 5×10^{-5} M oxidizing species, is compared in Figure 6 to the spectrum observed in similar solutions which were γ-irradiated with the same total dose. The similarity of the spectra indicates that the products in these two cases are identical or very similar. Since γ-irradiation will favor the formation of $(TMB)_2^{\bullet}$ via reaction 14 while the pulse conditions favor the formation of $(TMB)_2$ dimer via reaction 13, we conclude that the $(TMB)_2^{\bullet}$ radical eventually produces the $(TMB)_2$ dimer or a very similar species such as a trimer or tetramer of TMB in the very slow process 16.

Decay of $TMB^{\bullet+}$ above pH 9.2. Above pH 9, the decay of the transient absorption in the TMB solutions is rather more complicated. For as may be seen in Figure 7, for example, the single decay observed accounting for more than 90% of the total disappearance of the transient absorption at lower pHs is now divided into two stages well separated in time. Each of these stages represents more than one process. The fast stage consists of three decays marked I, II, and III in Figure 7, whereas the slow stage follows the same general kinetic behavior with respect to the mixed reaction order and the effect of pulse intensity as that observed below pH 9, although it is now faster and pH dependent. Table

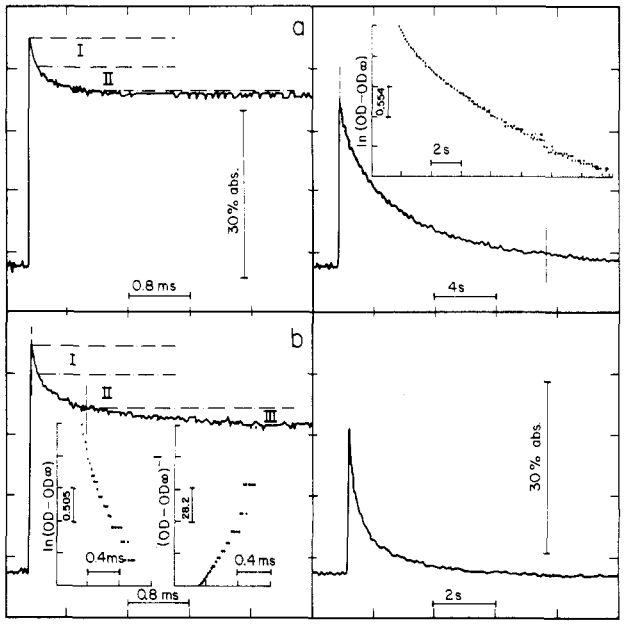

Figure 7. Typical decay curves for the absorption signals of $TMB^{\bullet+}$ in alkaline solutions: (a) [TMB] = 5×10^{-4} M, $[Br^-] = 2 \times 10^{-2}$ M, pH 10.1. Total radical concentration per pulse = 1.0×10^{-5} M, $G_{TMB^{\bullet+}} = 6$. (b) same conditions as in (a) except pH 11.1. Inserted plots demonstrate mixed kinetics.

SCHEME II

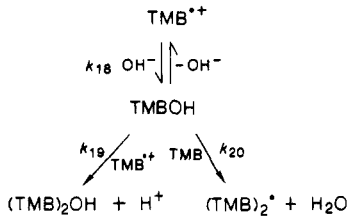

I summarizes the relevant experimental data for the decay of the transient signals above pH 9. We attribute the quite complex kinetic behavior observed for the overall decay of the $TMB^{\bullet+}$ signal at high pHs to the occurrence of the reactions given in Scheme II in addition to those given in Scheme I. It is suggested that $TMB^{\bullet+}$ is in equilibrium with the OH adduct TMBOH (eq 18) at high pHs and TMBOH may then react with either $TMB^{\bullet+}$ or TMB via reactions 19 and 20, respectively.

The three decays observed in the first stage of the overall decay may then be explained as follows. Decay I, representing 15% ± 2% of the total absorption signal, is observed in the whole pH range studied (3.5–11.1) and is attributed to reaction 15 between $TMB^{\bullet+}$ and TMBH. Decay II is probably related to acid–base equilibria in the OH/Br^- system.[18] We attribute decay III to the equilibration reaction 18 producing TMBOH. As the pH is raised the fraction of the signal disappearing via decay III increases (see Table I) and this is accounted for by the shift in equilibrium 18 producing greater amounts of TMBOH at higher pHs. The pH dependence of equilibrium 18 also affects the reactions occurring in the slow stage, for reactions 19 and 20 are fast in comparison with reactions 13 and 14, respectively. On raising the pH, therefore, the fraction of $TMB^{\bullet+}$ present in the form of TMBOH increases and hence the greater fraction of the slow stage of the decay via reactions 19 and 20 accounts for the enhancement of the rate of the slow stage with increasing pH. Although the rate constant of the bimolecular decay of TMBOH is relatively high, this reaction is not important under our conditions because of the low concentration of TMBOH relative to $TMB^{\bullet+}$.

(18) At higher pHs the pulse radiolytic behavior of Br^- solutions is quite complex (see, for example: Mamou, A.; Rabani, J.; Behar, D. *J. Phys. Chem.* **1976**, *81*, 1447) which may result in the formation of certain amounts of species other than $TMB^{\bullet+}$.

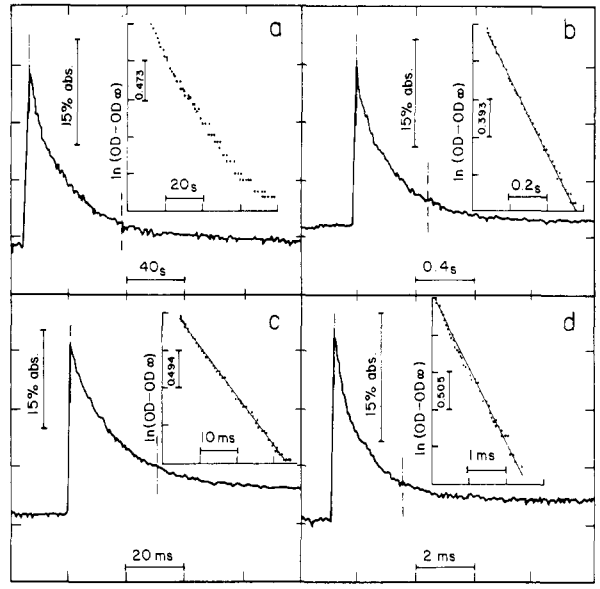

Figure 8. Decay of $DMB^{\bullet+}$ at various RuO_2 concentrations. [DMB] = 1×10^{-4} M, $[Tl^+] = 2 \times 10^{-3}$ M, pH 3.8. Total radical concentration per pulse = 1.4×10^{-5} M, $G_{DMB^{\bullet+}} = 2.4$. Wavelength = 460 nm: (a) No RuO_2; (b) 1×10^{-6} M RuO_2; (c) 1×10^{-5} M RuO_2; (d) 1×10^{-4} M RuO_2.

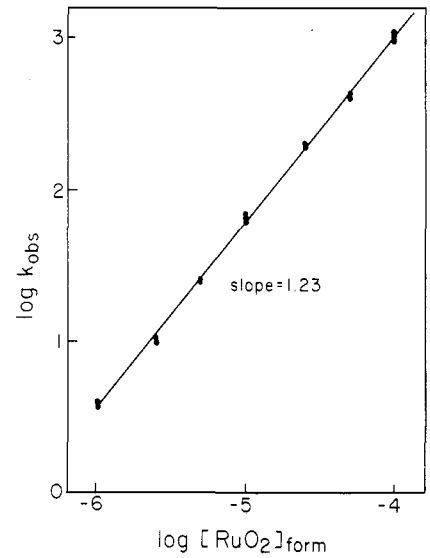

Figure 9. Catalytic decay of $DMB^{\bullet+}$. Pseudo-first-order rate constants measured under conditions such as in Figure 8 plotted vs. log $[RuO_2]_{form}$.

Part B: Disappearance of the Cation Radicals in the Presence of Colloidal RuO_2. The presence of colloidal RuO_2 does not affect, within the studied range of concentrations, the formation of the cation radicals although the absorption signals of $DMB^{\bullet+}$ at 460 nm and of $TMB^{\bullet+}$ at 447 nm are observed to decay according to first-order kinetics by several orders of magnitude faster than in the absence of RuO_2. It should also be noted that the presence of the stabilizing polymer alone (up to 0.1% concentration) shows no effect on the decay of either $DMB^{\bullet+}$ or $TMB^{\bullet+}$.

Decay of $DMB^{\bullet+}$. The decay of the $DMB^{\bullet+}$ absorption signal at pH 3.8 in the presence of colloidal RuO_2 was investigated at various wavelengths and over a wide range of catalyst concentrations. Considerable enhancements of the rate of decay could be observed, even at formal concentrations of catalyst as low as 1×10^{-6} M (see Figure 8) and it was found to be first order with respect to $DMB^{\bullet+}$. A small residual absorption was sometimes observed at the end of the decay (Figure 8d) although it was not investigated further. A plot of the logarithm of the observed rate constant for the decay vs. the logarithm of the formal RuO_2 concentration, $[RuO_2]_{form}$, as shown in Figure 9, indicates that the reaction possesses an order of 1.23 with respect to RuO_2, and

TABLE II: Effects of [RuO_2], pH, and Pulse Intensity on the Decay of $TMB^{\bullet+}$

pH	[TMB], 10^{-4} M	$[RuO_2]_{form}$, 10^{-5} M	pulse intensity,[a] 10^{-6} M	magn fast process,[b] 10^{-6} M	k_{fo},[c] s^{-1}	SO slope,[d] s^{-1}
2.8	5.0	6.0	12.0	4.1	94 ± 3	0.21 (0.37)
3.8[e]	5.0	6.0	7.7	4.2	108 ± 5	0.62 (0.63)
3.8[e]	5.0	6.0	12.6	4.5	164 ± 5	
3.8[e]	5.0	6.0	21.1	5.5	222 ± 6	
4.9	5.0	6.0	11.9	6.5	135 ± 5	0.50 (0.47)
6.1	5.0	6.0	11.6	7.3	80 ± 3	1.7 (0.49)
6.1	5.0	6.0	19.8	10.1	95 ± 3	
7.2	5.0	6.0	10.8	9.3	83 ± 3	
7.2	5.0	6.0	18.7	12.9	114 ± 5	9.9 (0.45)
7.4	2.0	0.30	8.6	1.4	20 ± 2	1.3 (0.25)
7.4	2.0	1.0	8.4	2.9	27 ± 2	2.1 (0.28)
7.4	2.0	3.1	11.7	8.0	43 ± 2	5.9 (0.34)
8.3	5.0	6.0	18.1	14.9	99 ± 3	
9.2	5.0	6.0	18.6	16.4	97 ± 3	
10.4	2.0	0.30	9.9		6 ± 1[f]	
10.4	2.0	1.0	10.2		13 ± 1[f]	
10.4	2.0	10.0	11.5	10.6	170 ± 5	

[a] Initial [$TMB^{\bullet+}$] minus [$TMB^{\bullet+}$] that reacted with TMBH, proportional to the pulse intensity. [b] In units of [$TMB^{\bullet+}$] that decayed in the faster process. [c] First-order rate constant for the fast decay obtained from plots of ln (OD − OD_∞) vs. time. See also text. [d] Initial slopes of plots of $(OD)^{-1}$ at 447 nm vs. time for the slower process. In parentheses are the calculated values according to eq 17. [e] Acetate buffer used to set the pH (see also Experimental Section). [f] Cf. Figure 13 and text for the meaning of k_{fo} in this case.

hence an empirical kinetic expression for the disappearance of DMB^+ is

$$\frac{-d[DMB^{\bullet+}]}{dt} = (8.7 \times 10^7)[RuO_2]_{form}^{1.23}[DMB^{\bullet+}] \quad (21)$$

Decay of $TMB^{\bullet+}$. The overall shape and time profile of the disappearance of the absorption signal of $TMB^{\bullet+}$ in the presence of RuO_2 was found to consist of several decays that were significantly dependent on the pH, [RuO_2], and pulse intensity. However, no effect of [TMB] was observed when it was varied by a factor of 2.5. In Figures 10–12 we present the effect of pH on the decay profiles of the optical absorbance signals in TMB solutions at various RuO_2 concentrations while numerical data summarizing the effects of RuO_2, pH, and pulse intensity on the decay of $TMB^{\bullet+}$ are given in Table II.

Up to four stages could be observed in the overall disappearance of the absorption signal of $TMB^{\bullet+}$, depending upon the experimental conditions used, and these are described in the following:

1. The first stage consists of between about 15% and 30% of the decay depending upon the pH and is complete within several hundred microseconds under our experimental conditions. This stage of the decay may be observed on the left-hand sides of Figures 11 and 12 and the decrease in the absorption signal due to this stage is represented by Δ. The time ranges in Figure 10 were too long for this decay to be observed. The fraction of $TMB^{\bullet+}$ decaying in this stage increases above about pH 9 as may be seen on comparing the data obtained in Figure 11 at pH 8 to that in Figure 12 at pH 10.4, although it remains independent of the RuO_2 concentration present as may also be seen in Figures 11 and 12. This rapid-decay stage is attributed to reaction of $TMB^{\bullet+}$ and TMBH (eq 15), which contributes ~15% of the total decay at all pHs, to the OH/Br^- equilibrium, and to the equilibrium between $TMB^{\bullet+}$ and TMBOH (eq 18), which accounts for the larger fractions of the total decay that occur during this stage at the higher pHs. These reactions all appear to take place in the bulk of the solution and have been discussed in detail in Part A of this study.

2. The second stage of the overall decay of the absorption signal of TMB^+ takes place in the time range of 10–200 ms, depending on the experimental conditions. This stage we call the "fast decay" in our discussion and it is clearly seen on the left-hand side of Figure 10 and on the right-hand sides of Figures 11 and 12. The amount of TMB^+ decaying in this stage is found to increase with both increasing pH (see left-hand side of Figure 10) and increasing [RuO_2] (see right-hand side of Figure 11).

This stage follows a first-order rate law as may clearly be seen from the inserts to the left-hand side of Figure 10 and the right-hand side of Figure 11. The rate of this stage is nearly independent of the pH, changing by less than a factor of 2 over the whole pH range studied at constant RuO_2 concentration. There is however a larger effect of [RuO_2] on the rate of the fast decay as may be seen for example on the right-hand side of Figure 12. The results are summarized in Figure 13 where the logarithm of the observed rate constant for the fast decay is plotted as a function of the logarithm of the RuO_2 concentration at pH 5, 8,

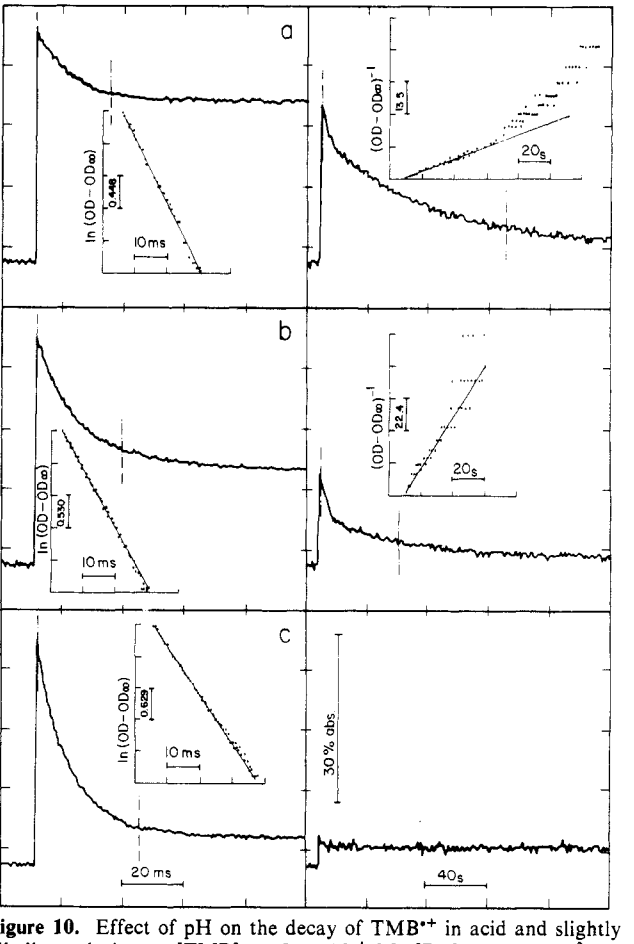

Figure 10. Effect of pH on the decay of $TMB^{\bullet+}$ in acid and slightly alkaline solutions. [TMB] = 5×10^{-4} M, [Br^-] = 2×10^{-2} M, $[RuO_2]_{form} = 6.0 \times 10^{-5}$ M. Total radical concentration per pulse = 1.4×10^{-5} M, wavelength = 447 nm. $G_{TMB^{\bullet+}} = 6$: (a) pH 3.0; (b) pH 6.1; (c) pH 8.3.

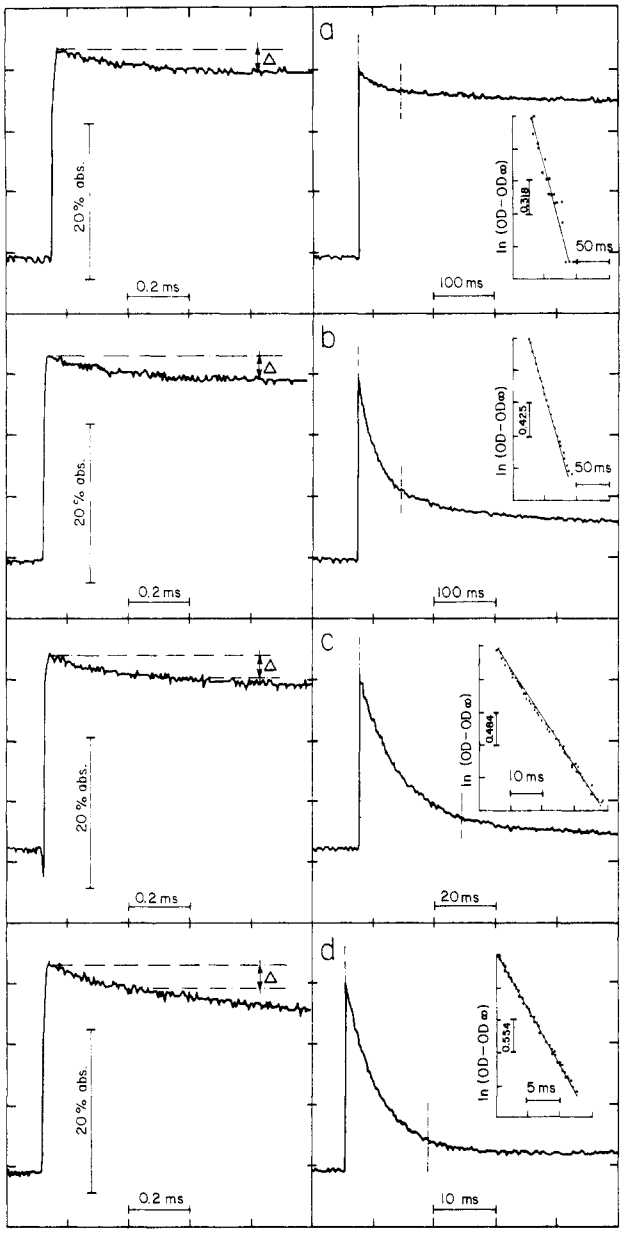

Figure 11. Effect of $[RuO_2]$ on the $TMB^{\bullet+}$ decay. [TMB] = 2×10^{-4} M, $[Br^-] = 2 \times 10^{-2}$ M, pH 8.0, total radicals/pulse = 1.1×10^{-5} M, $G_{TMB^{\bullet+}} = 6$: (a) $[RuO_2]_{form} = 1.5 \times 10^{-6}$ M; (b) $[RuO_2]_{form} = 1.6 \times 10^{-5}$ M; (c) $[RuO_2]_{form} = 5.0 \times 10^{-5}$ M; (d) $[RuO_2]_{form} = 1.2 \times 10^{-4}$ M. Δ denotes 15% ± 2% decay due to the reaction of $TMB^{\bullet+}$ with TMBH.

and 10.4. For pH 5 and 8 the observed rate constant for this stage remains practically unchanged below 3×10^{-5} M RuO_2 and then approaches a linear dependence on $[RuO_2]^{1.2}$ above this concentration of RuO_2. At pH 10.4 the observed rate constant is found to behave similarly with $[RuO_2]$ although it increases even at very low concentrations of RuO_2. This is probably since at this pH this stage of the overall decay cannot be easily resolved from the following stage as may be seen from the right-hand side of Figure 12, and hence the true values of k_{obsd} (marked by arrows in Figure 13) are probably considerably higher. It should be noted here that the dependency of the observed first-order rate constant on $[RuO_2]^{1.2}$ at high concentrations of RuO_2 indicates that this stage of the decay of $TMB^{\bullet+}$ follows the same form of kinetic rate law as that observed for the decay of $DMB^{\bullet+}$ (see eq 21).

The observed rate constant of the fast decay is also found to increase linearly with increasing pulse intensity at the lowest pHs investigated (pH 3–4) and at relatively low $[RuO_2]$. At higher pHs and $[RuO_2]$, under conditions where the fraction of $TMB^{\bullet+}$ decaying in the following stage approaches zero, no effect of pulse intensity is observed on the fast decay and indeed no effect of pulse intensity is observed for the highest $[RuO_2]$ used (2.4×10^{-4} M)

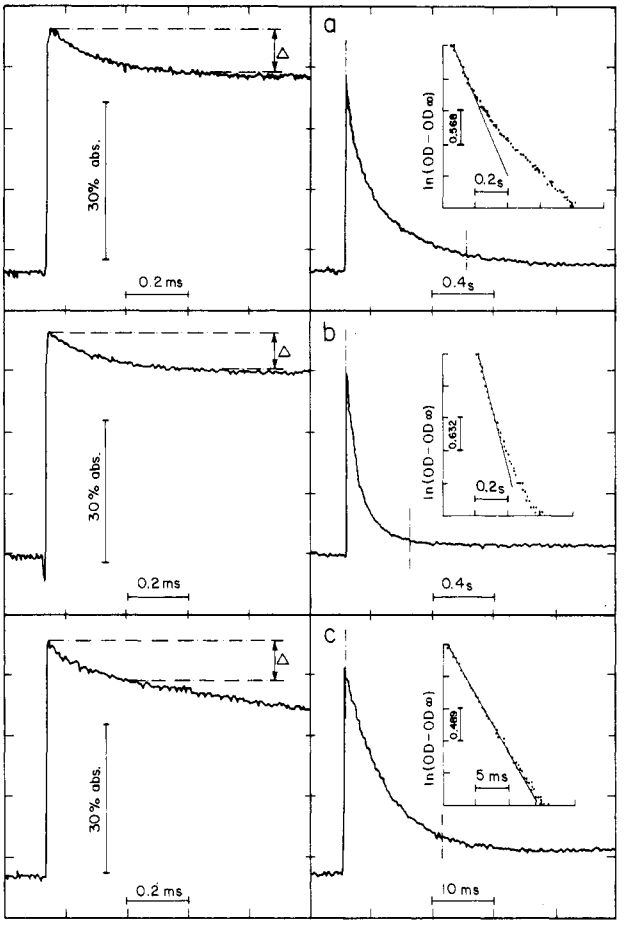

Figure 12. Fast and slow decays in alkaline solutions: [TMB] = 2×10^{-4} M, $[Br^-] = 0.02$ M, pH 10.4. Total radicals/pulse = 1.5×10^{-5} M, $G_{TMB^{\bullet+}} = 6$. (a) 3.0×10^{-6} M $[RuO_2]_{form}$; (b) 1.0×10^{-5} M $[RuO_2]_{form}$; (c) 1.0×10^{-4} M $[RuO_2]_{form}$. (c) 1.0×10^{-4} M $[RuO_2]_{form}$. Δ denotes an initial 30% ± 3% decay observed at pH ~10; cf. Figure 7a and the text.

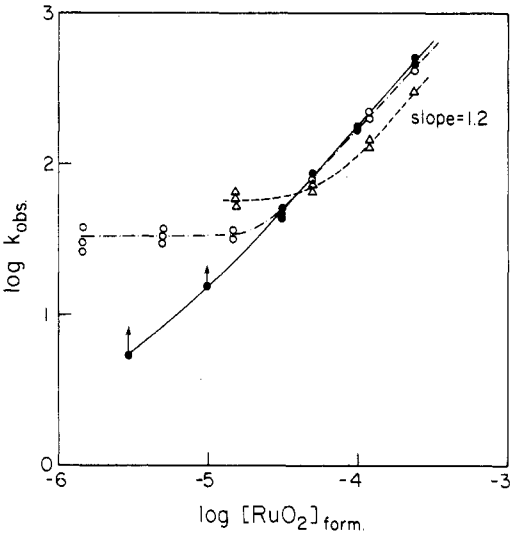

Figure 13. Fast decay of $TMB^{\bullet+}$. log k_{obsd} (pseudo-first order) plotted vs. log $[RuO_2]_{form}$ at various pHs: (●) pH 10.4; (○) pH 8.0; (△) pH 5.0. [TMB] = 5.0×10^{-4} M, $[Br^-] = 0.02$ M, radicals/pulse = 1.4×10^{-5} M.

at any pH. The changes between these two limiting conditions are gradual as may be seen in Table II.

3. The third stage of the decay, takes place in the second time range at low pHs, is clearly seen on the right-hand side of Figure 10. This stage is termed the slow decay in the remaining discussion. The fraction of $TMB^{\bullet+}$ decaying in this stage decreases with increasing pH and $[RuO_2]$ (see right-hand sides of Figures

SCHEME III

$$MB^{\bullet+}_{sol} \rightleftharpoons MB^{+}_{ads} \quad (22)$$

$$MB^{\bullet+}_{ads} \rightleftharpoons h^{+}_{ads} + MB_{sol} \quad (23)$$

$$mh^{+}_{ads} + OH^{-}_{sol} \rightleftharpoons OH^{(m-1)+}_{ads} \quad (24)$$

$$MB^{\bullet+} + OH^{(m-1)+}_{ads} \longrightarrow MBOH_{ads} + mh^{+}_{ads} \quad (25)$$

$$MB_{sol} + OH^{(m-1)+}_{ads} \longrightarrow MBOH_{ads} + (m-1)h^{+}_{ads} \quad (26)$$

$$2MBOH_{ads} \longrightarrow (MBOH)_{2ads} \quad (27)$$

$$(MBOH)_{2ads} \longrightarrow (MB)_{2sol} + 2H_2O \quad (28)$$

10 and 12) due to the corresponding increase in the fraction of $TMB^{\bullet+}$ decaying in the previous stage, and in our most extreme conditions of high pH and high $[RuO_2]$ this slow decay disappears completely.

Below pH ~5 the kinetics of the slow decay are identical with the decay of $TMB^{\bullet+}$ observed in the absence of RuO_2 and hence are attributed to reactions 13 and 14, which occur in the bulk of the solution. At higher pHs however a large enhancement in the rate of this decay is observed such that separation between the slow decay in this stage and the fast decay in the previous stage is not easily observed above pH 9. (See for exaple the right-hand side of Figure 12 at pH 10.4.) The existence of the slow decay at this pH is revealed however from the systematic deviations to the first-order plots of the fast decay. (See for example Figure 12a.)

4. The residual absorption observed after completion of the slow decay is approximately 10% of the initial absorption signal, and its fate depends also on pH and $[RuO_2]$. Its disappearance therefore constitutes the fourth stage in the overall decay of the $TMB^{\bullet+}$ absorption signal. At relatively low pHs and $[RuO_2]$ this residual absorption decays within about 30 min, similar to that observed in the absence of RuO_2, while at relatively high pHs and $[RuO_2]$ it is stable.

Analysis of O_2. No oxygen was detected after irradiation of reaction solutions in the presence of either DMB or TMB with or without RuO_2. An upper limit of $G(O_2) < 0.1$ may be estimated from experiments carried out with either repetitive electron pulses or γ-irradiation (maximum total absorbed dose was 30 krad). In the absence of DMB and TMB the presence of oxygen is detected, however, following irradiation of solutions of pH ≈ 11 when both Br^- and RuO_2 are present ($G(O_2) = 1.2$).[19]

Interpretation of the Results Obtained for the Decays of MB^+ in the Presence of RuO_2. The initial stage of decay of the absorption signal of MB^+ has already been attributed to reaction 15 (and also to equilibria 10 and 18 at the higher pHs) which occurs in the bulk of solution and hence we will focus our discussion on the second and third stages of the decay, namely the fast and slow decays, respectively.

A hole-loading model is proposed to account for the additional stages observed in the overall decay of the absorption signal of the methoxybenzene radical cations in the presence of RuO_2, and the reactions taking place with the colloid are summarized in Scheme III. The subscripts "sol" and "ads" represent the species present in solution and adsorbed onto the catalyst, respectively. Adsorption of $MB^{\bullet+}$ onto active sites on the colloid via equilibrium 22 is believed to occur followed by positive hole injection into the colloid via equilibrium 23. The holes produced reside on the catalyst at the higher pHs as $OH^{(m-1)+}_{ads}$, where m is the number of positive holes per OH^- adsorbed on the catalyst surface. The $OH^{(m-1)+}_{ads}$ species are then suggested to be scavenged by species such as $MB^{\bullet+}_{ads}$ or MB_{sol} to give the OH adduct adsorbed on the catalyst (eq 25 and 26), which then undergoes dimerization reactions to yield the final products (reactions 27 and 28). Our information on the nature of $OH^{(m-1)+}_{ads}$ is limited. It may contain a combination of h^+_{ads}, OH^-_{ads}, and/or OH_{ads}.

While we will apply the above mechanism in the following discussion principally to the decays observed with $TMB^{\bullet+}$ where a wide range of pH was studied, we do however believe that the same or a very similar model is also appropriate to describe the decay of $DMB^{\bullet+}$, which was only studied at acidic pHs. Evidence supporting this assumption will be given later.

Fast Decay. The fast decay of the absorption signal due to $MB^{\bullet+}$ is believed to occur because of the establishment of equilibria 22–24 in which hole loading of the catalyst particle by $MB^{\bullet+}$ leads to the overall formation of $OH^{(m-1)+}_{ads}$. The effects of pH, RuO_2, and pulse intensity on the magnitude and rate of the fast decay of the absorption signal of TMB^+ are all consistent with the hole-charging model.

The increase in the fraction of the overall disappearance of $TMB^{\bullet+}$ occurring in the fast decay with increase of pH above about pH 4 is attributed to the shift of equilibrium 24 to the right. However, below about pH 4 the amount of $TMB^{\bullet+}$ decaying in the fast decay remains almost constant at the same $[RuO_2]$ and pulse intensity (see Table II), suggesting that there is only a very small contribution of reaction 24 below this pH and hence only h^+_{ads} but no $OH^{(m-1)+}_{ads}$ is produced. The rate of the fast decay, which remains virtually independent of pH at constant $[RuO_2]$ over the whole pH range studied, probably suggests that reaction 22 or 23 controls the overall rate of establishment of the equilibrium depending upon the concentration of RuO_2 present.

At concentrations of RuO_2 above about 3×10^{-5} M where the rate and total amount of the fast decay both increase with increasing $[RuO_2]$, as has already been described in the results from Figures 11–13, the adsorption of $TMB^{\bullet+}$ ions on the catalyst, as given by eq 22, controls the position and rate of attainment of equilibrium. For as the $[RuO_2]$ is increased the number of active sites available for adsorption of $TMB^{\bullet+}$ increases and hence a greater number of collisions occur between $TMB^{\bullet+}$ cations and sites on the colloidal particles. At the low concentrations of RuO_2, where the rate of the fast decay of $TMB^{\bullet+}$ is found to be independent of $[RuO_2]$ (see Figure 13), saturation of the active sites by adsorbed $TMB^{\bullet+}$ is assumed to take place. In this case the observed rate constant of the fast decay is controlled by the rate of reaction 23, which is independent of the concentration of RuO_2.

The dependence of the loading rate constant on $[RuO_2]^{1.2}$ in both the DMB and TMB systems is not surprising. In other chemical systems involving loading of colloidal particles such as platinum and gold, deviations from first-order dependence on the catalyst have been reported[20] and in some cases even second-order dependence is observed.[21,22] In the system containing reduced methylviologen and colloidal platinum the reaction order was attributed to the necessity of reaction with exposed active sites on the colloid. It was originally suggested that they could be obtained by collisions between colloidal particles,[22] although more recently computer simulations of the reaction system have demonstrated that deviations from first-order dependence on catalyst concentration may occur as a result of adsorption of species on the catalyst particle surface.[23] The observed rate of the fast decay of DMB^+ is dependent on $[RuO_2]^{1.2}$ at RuO_2 concentrations as low as 1×10^{-6} M (see Figure 9), although such a dependence on $[RuO_2]$ is only found for the fast decay of TMB^+ at concentrations of RuO_2 above about 3×10^{-5} M (see Figure 13). This suggests that saturation of the active sites on the surface of the RuO_2 particles by $DMB^{\bullet+}$ is much more difficult to achieve than for $TMB^{\bullet+}$. This is probably related to the higher redox potential of $DMB^{\bullet+}$ as compared to that of $TMB^{\bullet+}$. For the position of equilibrium 23 is likely to be much further to the right for $DMB^{\bullet+}$ than for $TMB^{\bullet+}$, leading to much higher turnover rates for adsorbed $DMB^{\bullet+}$ as compared to adsorbed $TMB^{\bullet+}$.

Another feature of the fast decay that may be explained ac-

(19) The evolution of O_2 from the Br_2^- system in the presence of RuO_2 has been reported previously by: Dimitrievic, R. M.; Micic, O. I. *J. Chem. Soc., Dalton Trans.* **1982**, 1953. The authors investigated the reaction of Br_2^- with $Fe(bpy)_3^{2+}$ in the presence of a RuO_2 catalyst for water oxidation, but our results show that the presence of the iron complex is not necessary.

(20) Brandeis, M.; Nahor, G. S.; Rabani, J. *J. Phys. Chem.* **1984**, *88*, 1615.

(21) Meisel, D.; Mulac, W. A.; Matheson, M. S. *J. Phys. Chem.* **1981**, *85*, 179.

(22) Matheson, M. S.; Lee, P. C.; Meisel, D.; Pelizzetti, E. *J. Phys. Chem.* **1983**, *87*, 394.

(23) Sassoon, R. E.; Lenoir, P. M.; Kazak, J. J. *J. Phys. Chem.* **1986**, *90*, 4654.

cording to the proposed model is the dependency of the fast decay rate on pulse intensity. As noted earlier the independence of the rate constant for the fast decay on pH suggests that reaction 22 or 23 controls the rate of establishment of equilibrium. The linear increase in the pseudo-first-order rate constant with increasing pulse intensity in the pH range 3–4 is attributed to the fact that the adsorption process given by eq 22 is the rate-determining step since only a small fraction of $MB^{\bullet+}$ decays in this process at these pHs and not all the active sites on the catalyst surface are occupied. At the higher pHs, where the fast decay accounts for the entire decay of $TMB^{\bullet+}$, the pulse intensity has no observable effect on the rate of fast decay. Under such conditions all the active sites of the catalyst quickly become saturated with adsorbed species, causing reaction 23 to control the overall rate of fast decay, and hence a greater independence of the rate on the initial concentration of $TMB^{\bullet+}$ is observed.

Under all our experimental conditions the fast decays of both $DMB^{\bullet+}$ and $TMB^{\bullet+}$ follow good first-order kinetics (see Figure 8 and 10–12), in contrast to the methylviologen–colloidal platinum system where deviations from first-order dependency were observed as the loading of the platinum particles proceeded.[20] This may be attributed to the large negative charge of the polyelectrolyte stabilizer of the RuO_2 particles, which means that loading of the particles with positive holes may have only a small effect on their net charge.

It can be shown that if the loaded RuO_2 colloid is at equilibrium with the $TMB^{\bullet+}/TMB$ system at the end of the fast decay eq 29

$$\log [TMB^{\bullet+}]_{eq} = \log [TMB] - \frac{E^\circ_{TMB} - E^\circ_{RuO_2}}{0.0593} + \alpha(pOH) \quad (29)$$

represents the dependency of the equilibrium concentration of $TMB^{\bullet+}$, $[TMB^{\bullet+}]_{eq}$, on pOH. E°_{TMB} is the standard redox potential for the half-reaction $TMB^{\bullet+} + e^- \rightleftharpoons TMB$ and $E^\circ_{RuO_2}$ represents the apparent standard redox potential related to eq 30.

$$(RuO_2)_n(OH)_p^{2+} + e^- \rightleftharpoons (RuO_2)_n(OH)_{(p-\alpha)}^{(q-1+\alpha)+} + \alpha OH^- \quad (30)$$

Here $(RuO_2)_n(OH)_p^{q+}$ represents a RuO_2 colloidal particle, $(RuO_2)_n$, to which p OH^- ions are adsorbed and $(p - q)$ positive holes are loaded. It should be noted that the redox potential, $E^\circ_{RuO_2}$, depends on the degree to which hole loading takes place and on the degree that $(RuO_2)_n$ with a positive hole is accompanied by the uptake of OH^- according to eq 30 where $\alpha = 1/m$ and m is given in eq 24. The reduction potential for the $TMB^{+/0}$ couple in aqueous solution was measured to be +0.88 V vs. NHE and was found to be electrochemically reversible at scan rates between 20 and 2000 mV/s. This value, which is 0.18 V lower than that reported in acetonitrile solutions,[2] was used in our calculation of $E^\circ_{RuO_2}$.

The plots of log $[TMB^{\bullet+}]_{eq}$ vs. pOH for two pulse intensities are presented in Figure 14. The linear parts of the figure are in accordance with eq 29, yielding $\alpha = (0.22 \pm 0.02)$, and hence it appears that the loading of around every four positive holes requires the adsorption of one OH^- ion. Average values of $E^\circ_{RuO_2}$ of ~0.68 and ~0.65 V are obtained from the graphs of Figure 14 for total $[TMB^{\bullet+}]$ produced per pulse of 2.1×10^{-5} M and 1.2×10^{-5} M, respectively. The difference between these two values of $E^\circ_{RuO_2}$ is probably due to differences in the average number of positive holes loaded per colloid particle which is higher at the higher pulse intensity. The leveling off of the graphs below the limiting values observed below pH 5 shows that loading of the colloid particles takes place even at these low pHs. Here hole loading probably occurs just via reaction 23 without the uptake of any OH^- ions. The redox potential of $(RuO_2)_n$ is then pH independent and the concentration of $TMB^{\bullet+}_{eq}$ remains constant with pH.

It should be noted that the values of $E^\circ_{RuO_2}$ given above for the colloidal particles cannot be related directly to the electrochemical properties of RuO_2 electrodes, which are known to possess metallic characteristics. For although relatively little is known about the structure and properties of colloidal RuO_2 in water, there is some evidence that such particles may exist in a hydroxylated

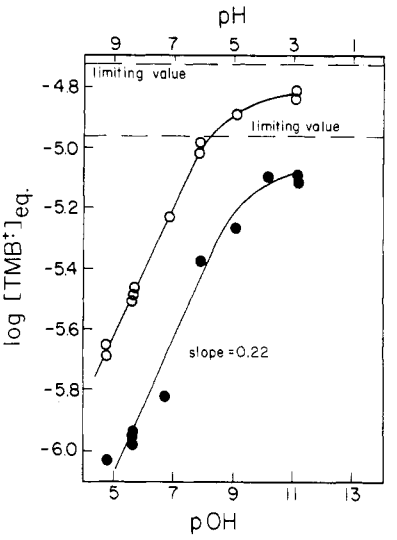

Figure 14. Dependence of $[TMB^{\bullet+}]_{eq}$ on pH. [TMB] = 5×10^{-4} M, $[Br^-] = 2 \times 10^{-2}$ M, $[RuO_2]_{form} = 6.0 \times 10^{-5}$ M. (●) Total radicals/pulse = $(1.3 \pm 0.1) \times 10^{-5}$ M. (○) Total radicals/pulse = $(2.3 \pm 0.1) \times 10^{-5}$ M.

form and the possibility that the colloid contains some trivalent ruthenium can also not be excluded.[24] Furthermore, whereas the RuO_2 electrode acts as a virtually infinite sink for charge loading, colloidal RuO_2 on the other hand contains only a limited number of sites that may be loaded with holes and hence a value of $E^\circ_{RuO_2}$ may be assigned to the colloid, which of course depends upon its properties and upon the degree to which it is loaded.

It should further be emphasized that the pH effects agree with a hole-loading mechanism. The results cannot be understood in terms of a pH-dependent adsorption of the $TMB^{\bullet+}$ followed by a dimerization or other decomposition reaction on the surface of the colloid to yield final products without the need to obtain charge injection into the colloid. While adsorption of OH^- may occur on unloaded RuO_2 and may in some cases be the first stage of reaction 24, such a reaction alone cannot explain the virtual independence of the experimentally observed rate constants for the fast decay of $TMB^{\bullet+}$ on pH particularly at high RuO_2 concentrations as may be seen in Figure 13. Furthermore the effect of pulse intensity when analyzed quantitatively (Figure 14) is too large to be accounted for solely by an OH^- adsorption model, and moreover the results of Figure 14 would imply that each OH^- ion adsorbed on the RuO_2 colloid facilitates adsorption of four $TMB^{\bullet+}$ radical cations, which also appears unreasonable. We therefore believe that we have convincing evidence that a hole-charging mechanism of the type given in Scheme III is correct for the behavior of $TMB^{\bullet+}$ with colloidal RuO_2.

Slow Decay. The slow decay of the absorption signal of TMB^+, which occurs after equilibria 22–24 are established, is attributed to reactions occurring in the bulk of solution at acidic pHs and to reactions 25 and 26 in Scheme III at higher pHs. In the pH range 3–5 the rate of the slow decay is comparable to that in the absence of RuO_2 when normalized to the same initial $TMB^{\bullet+}$ (Table II). Thus under these conditions the methoxybenzene radical cation decays in the solution via reactions 13 and 14. Above pH 5 reactions 25 and 26 become important as the $OH_{ads}^{(m-1)+}$ produced in the fast decay is scavenged by TMB and $TMB^{\bullet+}$. Decay of the absorption signal due to TMB^+ is then observed because of the direct disappearance of TMB^+ in reaction 25 and also the shift in equilibria 22–24 to the right as $OH_{ads}^{(m-1)+}$ is consumed in reactions 25 and 26. Both the pH and RuO_2 effects on the rate of the slow decay are then explained by the increasing amounts of $OH_{ads}^{(m-1)+}$ at the higher pHs and RuO_2 concentrations leading to faster rates of reactions 25 and 26.

The lack of oxygen formation in these systems in the presence of RuO_2 even though both $DMB^{\bullet+}$ and, at the higher pHs, $TMB^{\bullet+}$

(24) Heller, A., private communication.

possess redox potentials sufficient for water oxidation can now clearly be understood. Reactions 25 and 26, which involve scavenging of the loaded oxidized species, $OH_{ads}^{(m-1)+}$, on the catalyst, compete totally with any further reaction of these species yielding oxygen from water.

The residual absorption formed at the end of the slow decay is attributed to the formation of dimeric species of the OH adduct such as that given in eq 27, and any further decays in the time range of minutes are probably related to the formation of more stable dimeric products such as MB_2 as shown in eq 28.

Most of the above discussion has been concerned with the results obtained with TMB in the presence of RuO_2, but we believe a similar hole-loading mechanism applies also to DMB for the following important reasons. First, the rate law for the decay of $DMB^{\bullet+}$ in the presence of RuO_2 is virtually identical with that for the fast decay of $TMB^{\bullet+}$ at the higher RuO_2 concentrations. Second, the redox potential of DMB is considerably higher than that of TMB, suggesting that hole loading is even more favored for DMB than for TMB. This is indeed seen where the dependence of the rate of fast decay on $[RuO_2]^{1.2}$ is observed at much lower concentrations of RuO_2 for DMB and is attributed to the greater ability of $DMB^{\bullet+}$ to inject RuO_2 with positive holes as compared to $TMB^{\bullet+}$.

Conclusions

In this investigation we have used the technique of pulse radiolysis to probe the mechanism by which oxidized species react with a ruthenium dioxide colloidal catalyst. From the pH effects observed we have clearly shown that a hole-loading process is involved. At present, it appears that methoxybenzenes are ineffective as mediators in O_2 generation from water because of their tendency to scavenge the positive holes on the catalyst surface. However, because of their high redox potentials, they may have potential use as "relay" molecules in various types of photochemical and photogalvanic systems.

It is now evident that not all good electron-donor species with high redox potentials will necessarily produce oxygen from water in the presence of a colloidal catalyst such as RuO_2. Side reactions on the catalyst surface, such as the formation of OH adducts, must also be inhibited and the search for more suitable candidates for water oxidation is continuing.

Acknowledgment. This work was supported by the Balfour and Schrieber Foundations and by the USA-Israel BSF.

Registry No. DMB, 150-78-7; TMB, 2441-46-5; $DMB^{\bullet+}$, 34478-03-0; $TMB^{\bullet+}$, 34515-61-2; $(DMB)_2$, 61181-04-2; $(TMB)_2$, 105102-76-9; RuO_2, 12036-10-1; Tl^{2+}, 14700-72-2; Br_2, 7726-95-6; H_2O, 7732-18-5.

Relaxation Time Measurements in *N*-(1-Butyl)pyridinium–Aluminum Chloride Ambient Temperature Ionic Liquids

Thomas A. Zawodzinski, Jr., Robert Kurland,† and R. A. Osteryoung*

Department of Chemistry, State University of New York, Buffalo, New York 14214
(Received: February 10, 1986)

Proton spin-lattice relaxation times (T_1) have been determined for the protons attached to the butyl moiety on the *N*-(1-butyl)pyridinium cation present in the room temperature molten salt system composed of mixtures of aluminum chloride with *N*-(1-butyl)pyridinium chloride at various mole ratios. Reorientational correlation times have been estimated from the data. From the viscosity dependence of these correlation times for protons in various positions on the butyl chain, it is shown that strong cation–anion interactions occur only when chloride anion is present in the melt. Also, the field dependence of the relaxation times has been analyzed to yield correlation times for the random motion giving rise to a relaxation mechanism. The behavior of these experimentally derived correlation times with melt composition and viscosity suggests the following: in acidic melts both overall rotation and internal motion contribute to the relaxation of the alkyl chain protons, while in basic melts, the motion in the terminal methyl group protons is effectively uncoupled from the overall rotation of the $BuPy^+$ cation.

Introduction

Molten salts composed of mixtures of $AlCl_3$ with *N*-alkylpyridinium halides or other organic halides are liquids at or below room temperature, often over a wide range of composition. These ionic liquids have been subjected to a variety of spectroscopic and electrochemical studies.[1-6] In particular, data from ^1H and ^{13}C NMR and other studies have been the basis for models for melt structure involving ion pairs or larger aggregates. Variations in chemical shifts of the organic cation have been ascribed to an anion interacting electrostatically with the organic cation. Models were proposed in which ion pairs[6] or aggregates[4] were taken as significant local structures; the models were tested by a fit of the data to a random statistical distribution of possible combinations of the various anions present in the melt in the structural unit considered. The chemical shifts for monomeric or dimeric species were taken from shifts determined experimentally at certain melt compositions in which only one anionic species was present. Thus, the test of the models was indirect.

When a particular type of interaction dominates the relaxation of an NMR active nucleus, measurement of the relaxation times can be used to obtain information on the motional characteristics of the molecule to which the nucleus is attached. For instance, carbon-13 NMR has been widely used to investigate the rotation of organic species in solution, based on the dominance of the intramolecular dipole–dipole interaction as a relaxation mechanism for carbon atoms with directly attached protons.[7] Proton relaxation times are less widely used in this type of investigation due to complications involved in separating the intramolecular component of the relaxation times from intermolecular contributions. An additional difficulty in analyzing proton relaxation

† Present address: Department of Special Imaging—Radiology, Geisinger Medical Center; 29-00, Danville, PA 17822.

(1) Robinson, J.; Bugle, R. C.; Chum, H. L.; Koran, D.; Osteryoung, R. A. *J. Am. Chem. Soc.* **1979**, *101*, 3776.
(2) Tait, S.; Osteryoung, R. A. *Inorg. Chem.* **1984**, *23*, 4352.
(3) Lipsztajn, M.; Osteryoung, R. A. *J. Electrochem. Soc.* **1985**, *132*, 1126.
(4) Fannin, A. A., Jr.; King, L. A.; Levisky, J. A.; Wilkes, J. S. *J. Phys. Chem.* **1984**, *88*, 2609.
(5) Nanjundiah, C.; Shimizu, K.; Osteryoung, R. A. *J. Electrochem. Soc.* **1982**, *129*, 2474.
(6) Taullelle, F.; Popov, A. *Polyhedron* **1983**, 889.
(7) Levy, George C. *Acc. Chem. Res.* **1973**, *6*, 161.

0022-3654/87/2091-0962$01.50/0